Accepted Manuscript

Catalase-loaded cisplatin-prodrug-constructed liposomes to overcome tumor hypoxia for enhanced chemo-radiotherapy of cancer

Rui Zhang, Xuejiao Song, Chao Liang, Xuan Yi, Guosheng Song, Yu Chao, Yu Yang, Kai Yang, Liangzhu Feng, Zhuang Liu

Catalase-Loaded Cisplatin-Prodrug-Constructed Liposomes to Overcome Tumor Hypoxia for Enhanced Chemo-Radiotherapy of Cancer

Rui Zhang[1], Xuejiao Song[1], Chao Liang[1], Xuan Yi[2], Guosheng Song[1], Yu Chao[1], Yu Yang[1], Kai Yang[2], Liangzhu Feng[1]*, Zhuang Liu[1]*

Ms. R. Zhang, Ms. X.J. Song, Mr. C. Liang, Dr. G.S. Song, Mr. Y. Chao, Mr. Y. Yang. Prof. L.Z. Feng, Prof. Z. Liu, Institute of Functional Nano & Soft Materials (FUNSOM), Jiangsu Key Laboratory for Carbon-Based Functional Materials & Devices, Soochow University, Suzhou 215123, China

E-mail: zliu@suda.edu.cn, lzfeng@suda.edu.cn

Mr. X. Yi, Prof. K. Yang, School of Radiation Medicine and Protection & School for Radiological and Interdisciplinary Sciences (RAD-X), Medical College of Soochow University, Suzhou, Jiangsu 215123, China

Key words: chemo-radiotherapy, liposome, cisplatin prodrug, catalase, tumor hypoxia

Aiming at improved therapeutic efficacies, the combination of chemotherapy and radiotherapy (chemo-radiotherapy) has been widely studied and applied in clinic. However, the hostile characteristics of tumor microenvironment such as hypoxia often limit the efficacies in both types of cancer therapies. Herein, catalase (CAT), an antioxidant enzyme, is encapsulated inside liposomes constituted by cisplatin(IV)-prodrug-conjugated phospholipid, forming CAT@Pt(IV)-liposome for enhanced chemo-radiotherapy of cancer. After being loaded inside liposomes, CAT within CAT@Pt(IV)-liposome shows retained and well-protected enzyme activity, and is able to trigger decomposition of H_2O_2 produced by tumor cells, so as to produce additional oxygen for hypoxia relief. As the result, treatment of CAT@Pt(IV)-liposome induces the highest level of DNA damage in cancer cells after X-ray radiation compared to the control groups. In vivo tumor treatment further demonstrates a remarkably improved therapeutic outcome in chemo-radiotherapy with such CAT@Pt(IV)-liposome nanoparticles. Hence, an exquisite type of liposome-based nanoparticles is developed in this work by integrating cisplatin-based chemotherapy and catalase-induced tumor hypoxia relief together for combined chemo-radiotherapy with great synergistic efficacy, promising for clinical translation in cancer treatment.

1. Introduction

Chemotherapy and radiotherapy are two mainstream cancer treatment modalities in clinic for various types of cancers [1-3]. However, severe side effects and inducible resistance associated with those conventional cancer therapies have made them difficult to satisfy the clinical requirements, obliging scientists to develop new strategies in cancer treatments. The chemo-radiotherapy, which is delivered by concurrent administration of chemotherapy and radiotherapy, has received tremendous interests in both basic research and clinical trials, aiming at improving therapeutic outcomes for tumor patients [4-6]. It is known that the chemotherapy in the concurrent chemo-radiotherapy could not only act as a radiosensitizer to promote radiotherapy efficacy, but also potentially eradicate those distant micro-metastases spared from the radiation beam exposure, leading to synergistic treatment outcomes especially for those advanced cancer patients [7-9].

However, like many other cancer therapeutics, chemo-radiotherapy is also not omnipotent to any types of cancers [10-12]. Similar to single radiotherapy, which needs sufficient molecular oxygen to stabilize radiation-induced DNA breaks and shows limited efficacy to kill tumor cells in the hypoxic regions within solid tumors, the therapeutic efficacy of chemo-radiotherapy has also been found to be significantly hindered by tumor hypoxia, a hostile characteristics of most solid tumors [13-17]. Recently, tumor hypoxia relief has been demonstrated to be a rather promising strategy for improved cancer radiotherapy [18-26]. Apart from increasing the tumor reoxygenation by the normalization of tumor vasculature or intratumoral oxygen delivery with artificial blood substitutes (e.g. perfluorocarbon) to overcome hypoxia-associated radiation resistance, several different groups including ours have uncovered that the decomposition of endogenous hydrogen peroxide (H_2O_2) inside the tumor with specific catalysts could be an alternative strategy for effective

tumor reoxygenation [27-33]. More recently, we found that catalase, an enzyme that could decompose H_2O_2 into H_2O and O_2, could be efficiently encapsulated inside tantalum oxide (TaO_x) nanoshells, obtaining catalase loaded TaO_x nanoshells to efficiently relieve the tumor hypoxia by decomposing tumoral endogenous H_2O_2, subsequently leading to greatly improved cancer radiotherapy [34]. To date, however, efficient cancer chemo-radiotherapy with tumor hypoxia relief, preferable delivered by biocompatible nano-carriers, remains to be developed to our best knowledge.

Cisplatin, one of several robust chemotherapy drugs for efficient cancer chemo-radiotherapy in clinic, has recently been found to be able to be easily oxidized to cisplatin prodrug (cisplatin(IV)) by introducing two additional axial ligands for the purpose of decreasing cisplatin associated side effects [9, 35, 36]. In a recent work by our group, we uncovered that cisplatin(IV) pro-drug conjugated phospholipid together with other commercial lipids could easily form Pt(IV)-liposomes, which showed efficient tumor passive accumulation after intravenous (i.v.) injection [37]. To uncover whether tumor hypoxia relief could efficiently improve the therapeutic efficacy of chemo-radiotherapy, in this work, water soluble catalase (CAT) is encapsulated inside the liposomes formed with cisplatin (IV) pro-drug conjugated 1,2-distearoyl-sn-glycero-3-phosphoethanolamine (Pt(IV)-DSPE), 1,2-dipalmitoyl-snglycero-3-phosphocholine (DPPC), cholesterol, and polyethylene glycol (PEG) conjugated DSPE (DSPE-mPEG$_{5k}$) (**Figure 1**). It is found that catalase loaded inside such CAT@Pt(IV)-liposome shows retained and well-protected enzyme activity. As a result, such CAT@Pt(IV)-liposome induces the most effective DNA damage after being concurrently treated with X-ray radiation under the hypoxic condition. Like other PEGylated stealth liposomes, our CAT@Pt(IV)-liposome after i.v. injection shows efficient passive accumulation in tumors, in which the hypoxic status could be obviously relieved. Thereafter, the in vivo combined chemo-radiotherapy

with CAT@Pt(IV)-liposome results in the most effective inhibition effect on tumor growth.

2. Experimental Section

2.1．Materials

Catalase solution (≥35,000 units/mg protein) was purchased from Aladdin. Cisplatin was purchased from Beijing ZhongShuo Pharmaceutical Technology Development Co., Ltd. DSPE and DPPC were purchased from Xi'an Ruixi Biological Technology Co., Ltd. DSPE-mPEG$_{5k}$ was purchased from Laysan Bio Inc. Cholesterol was purchased from *J&K* Scientific Ltd. N-(3-Dimethylaminopropyl)-N-ethylcarbodiimide hydrochloride crystalline (EDC), N-Hydroxysuccinimide (NHS), and 3-(4,5-dimethylthiazol-2-yl)-2,5-diphenyl-tetrazolium bromide (MTT) were all purchased from Sigma-Aldrich. RPMI-1640 medium and fetal bovine serum (FBS) were purchased from Thermo Fisher Scientific Inc. All other chemicals were purchased from China National Pharmaceutical Group Corporation and used without further purification.

2.2．Preparation of liposomes

The DSPE-Pt(IV) was synthesized according to our previously developed method [37]. The dried lipid mixture of DSPE-Pt(IV) (16.66 mg), DPPC (10.48 mg), Cholesterol (2.87mg) and DSPE-mPEG$_{5k}$ (5 mg) at the molar ration of 8 : 8 : 4 : 1 were firstly dissolved in 1 ml chloroform and then dried under vacuum. Afterwards, the dried lipid was dispersed in 2 mL phosphate buffered saline (PBS) containing 3 mg CAT (mass ratio: Pt : CAT = 0.9) for hydration. After being extruded through a 200 nm polycarbonate filter for 20 times, excess CAT was removed from liposomes by Sephacryl S-300 high resolution column (GE Healthcare).

2.3．Liposome characterization

The dynamic light scattering (DLS) measurement was carried out with a Malvern Zetasizer (Nano Z90). The morphology of CAT@Pt(IV)-liposome was observed under a TEM (Tecnai F20, FEI) after staining liposomes by phosphotungstic acid (1 wt.%) according to the standard procedure. The encapsulation efficiency of CAT was measured by using the standard bicinchoninic acid (BCA) protein assay (Thermo Scientific). The concentration of cisplatin was measured by recording the concentration of Pt using an inductively-coupled plasma atomic-emission spectroscopy (ICP-AES, Thermo).

2.4．Evaluation of Catalase activity

The catalytic activities of free CAT and CAT@Pt(IV)-liposome were measured using the standard Góth's method [34, 38]. Briefly, free CAT and CAT@Pt(IV)-liposome were added into 0.5 mL H_2O_2 solution (50 mM) and reacted at 37 ^{o}C for 1 min. Then, the reaction was terminated by adding 0.5 mL ammonium molybdate (32.4 mM) by reacting with the residual H_2O_2 to form stable primrose yellow complexes. After being cooled down to 25 ^{o}C, the absorbance of each sample at 400 nm was measured with a UV-vis spectrometer (Genesys 10S, Termo). The relative catalytic activity was calculated by using the following equation: relative catalytic activity = (absorbance of H_2O_2 with PBS - absorbance of H_2O_2 with CAT@Pt(IV)-liposome) / (absorbance of H_2O_2 with PBS - absorbance of H_2O_2 with free CAT).

To determine the stability of free CAT and CAT@Pt(IV)-liposome against protease digestion, both free catalase and CAT@Pt(IV)-liposome samples at a CAT concentration of 10 μg mL^{-1} were mixed with protease K at a concentration of 0.5 mg mL^{-1} and kept at 37 ^{o}C. At designated time intervals, the catalytic activity of each sample was measured following aforementioned Góth's method.

Additionally, the portable dissolved oxygen meter was used to evaluate the catalytic activity of CAT@Pt(IV)-liposome at a series of concentrations by recording the dissolved oxygen concentration in the H_2O_2 solution (1 mM).

2.5．Cell experiments

4T1 murine breast cancer cells were obtained from American Type Culture Collection (ATCC) and cultured in RPMI-1640 cell culture medium supplemented with 10% FBS and 1% penicillin/streptomycin under the humidified atmosphere at 37 ^{o}C.

To test the cytotoxicity of CAT@Pt(IV)-liposome, 4T1 cells pre-seeded in 96 well plates were incubated with CAT@Pt(IV)-liposome, Pt(IV)-liposome, free cisplatin or CAT at a series of concentrations for 48 h. After that, the relative cell viability of each sample was evaluated by using the standard MTT assay.

To study the cell uptake profile of CAT@Pt(IV)-liposome, CAT was firstly labeled with fluorescein (Thermo) and then used to fabricate FITC-CAT@Pt(IV)-liposome. For confocal fluorescence imaging, 4T1 cells were incubated with FITC-CAT@Pt(IV)-liposome (Pt, 15 μg mL^{-1}) for 2 h, washed with PBS, and then further incubated within fresh cell culture medium containing Lyso-tracker Red (Invitrogen) (100 nM) for lysosome staining. After 1 h incubation, those cells was washed twice with PBS, fixed with 4% paraformaldehyde, stained with 4,6-diamino-2-phenylindole (DAPI), and then observed under the confocal laser scan microscopy (CLSM, Leica TCS-SP5II, Germany). The wavelength of the excitation lasers and emission filters used in CLSM observation were 405-nm excitation and 430~550 nm emission for DAPI, 488-nm excitation and 500~535 nm for FITC, as well as 543-nm excitation and 555~620 nm emission for Lyso-tracker, respectively.

To evaluate DNA damage post different treatments under a hypoxic condition, the double strand

break status of those 4T1 cells were visualized using the CLSM to record the fluorescence signals of γ-H2AX, a well-known marker of DNA double stand break. In brief, cells cultured under a hypoxic condition (5% CO_2 / 1% O_2 / 94 %N_2) were incubated with CAT@Pt(IV)-liposome, Pt(IV)-liposome and CAT@ liposome (Pt: 15 μg mL^{-1}, catalase: 9 μg mL^{-1}) for 2 h, and then exposed to the RS-2000 Pro Biological Irradiator (160 kV, 25 mA, Radsource) at a dose of 6 Gy. After another 1 h incubation, the cells were washed with PBS and fixed with 4 % paraformaldehyde for 10 min followed by PBS washing and being permeabilized with 0.2 % Triton X-100 solution for 10 min at room temperature. Afterwards, those cells were rinsed by PBS again, and then incubated with a blocking buffer (1 % bovine serum albumin, BSA) and 0.2 % Triton X-100 in PBS) for 1 h at room temperature before being stained with anti-phospho-histone γ-H_2AX mouse monoclonal antibody (dilution: 1 : 1000) (Abcam, UK) overnight at 4°C. On the second day, the cells were equilibrated to room temperature, washed with PBS, and then incubated with Cy3-conjugated sheep anti-mouse secondary antibody (dilution: 1 : 1000) for 1 h at 37 °C. Afterwards the cells were washed with PBS again, stained with DAPI and imaged by the CLSM. The wavelength of the excitation lasers and emission filters used in CLSM were 405-nm excitation and 430~550 nm emission for DAPI, as well as 543-nm excitation and 555~620 nm emission for Cy3, respectively. Quantitative analysis of γ-H2AX foci density (foci/100 μm^2) was conducted automatically using the ImageJ software for 100 cells in each treatment group.

For clonogenic assay, different number of 4T1 cells were seeded in 6-well plates and cultured at 37 °C overnight. Then, these cells were treated with CAT@liposome (18 μg mL^{-1}) in the presence of 50 μM H_2O_2 for 2 h under the hypoxic condition (5% CO_2 / 1% O_2 / 94 % N_2), followed by being exposed to X-ray radiation (photon energy of 140 keV) at doses of 0 Gy, 2 Gy, 4 Gy and 6 Gy,

respectively. The cells of control group were treated under the same parameters apart from without addition of CAT@Liposome. 1 h later, cells were washed with PBS and cultured in fresh cell culture medium at 37 °C under 5 % CO_2 for another 7 days. After that, those cells were fixed with methanol and stained with Giemsa for surviving fraction statistics according to the standard method [34].

2.6．Animal experiments

Female Balb/c mice were bought from Nanjing Sikerui Biological Technology Co. Ltd. All animal experiments were conducted following the animal protocols approved by the laboratory animal center of Soochow University. For tumor inoculation, 50 μL 4T1 cells solution (2×10^6 cells) was subcutaneously injected onto the back of each mouse to develop the tumor model.

For in vivo fluorescence imaging, three tumor-bearing mice received an i.v. injection of CAT@Pt(IV)-liposome (Pt: 3.3 mg kg^{-1}, catalase: 2 mg kg^{-1}) labeled with a lipophilic dye, 1,1'-dioctadecyl-3,3,3',3'-tetramethylindodicarbocyanine (DiD) were then imaged under a Maestro in vivo optical imaging system (Cambridge Research & Instrumentation, Inc) at different time intervals. At 36 h post injection (p.i.), the mice were sacrificed, and the main organs were collected and imaged. The fluorescence intensity was analyzed by Maestro software.

To evaluate the tumor hypoxia evolution post various treatments, 12 Balb/c mice bearing 4T1 tumors were i.v. injected with CAT@Pt(IV)-liposome, Pt(IV)-liposome, CAT@liposome or saline (three mice per group, Pt: 3.3 mg kg^{-1}, catalase: 2 mg kg^{-1}). At 24 h p.i., each mouse was i.p. injected with pimonidazole hydrochloride (30 mg kg^{-1}) (Hypoxyprobe-1 plus kit, Hypoxyprobe Inc) according to the procedure provided by the manufacture. 1.5 h later, the mice were sacrificed to collect tumor slices for immunofluorescence staining by adopting our previously used experimental procedure [30, 34]. Finally, the slices were observed using the CLSM. The tumor hypoxia status was

semi-quantitatively analyzed using the ImageJ software, and the positive hypoxia area was calculated with the following equation: The hypoxia positive area (%) = the area of fluorescence of hypoxia marker / total area (n = 10 images/group).

For in vivo combination therapy, 35 tumor-bearing mice were randomly divided into 7 groups (5 mice per group) as follows: I) control group with PBS injection only; II) bare chemotherapy group with Pt(IV)-liposome injection only; III) CAT@Pt(IV)-liposome injection only; IV) bare radiotherapy group with X-ray exposure only; V) Pt(IV)-liposome injection plus X-ray exposure; VI) CAT@liposome injection plus X-ray exposure; VII) CAT@Pt(IV)-liposome injection plus X-ray exposure. When the tumor volume of mice reached about 200 mm^3, all mice were received twice i.v. injection of various different drugs as indicated at day -1 and day 2 and then exposed to X-ray radiation (6 Gy) at 24 h p.i. if needed. The doses of Pt and catalase were 3.3 mg kg^{-1} and 2 mg kg^{-1}, respectively. Since day 0, the length and width of each tumor were measured by a digital caliper every 2 days for 14 days. The tumor volume was calculated following a standard formula: volume = width^2 × length/2. The growth curve was calculated by comparing the tumor volumes (V) at all days to the initial tumor volumes at day 0 (V_0). To evaluate the therapeutic effect of each treatment group, one mouse from each group was sacrificed 4 days after treatments were initiated to collect the tumors for H&E staining.

3. Results and Discussion

3.1. Preparation and characterization of CAT@Pt(IV)-liposome Owing to their great biocompatibility, excellent pharmacokinetic profiles and versatile drug loading abilities,

liposome-based drug carriers have been extensively explored in the past few decades [39]. Herein, to study the potential synergistic therapeutic effect of tumor hypoxia relief and chemo-radiotherapy, the CAT@Pt(IV)-liposome was prepared by hydrating the dried lipid film composed of Pt(IV)-DSPE, DPPC, cholesterol and DSPE-mPEG$_{5k}$ at a molar ratio of 8 : 8 : 4 : 1 in the PBS containing catalase following standard procedures to prepare liposomes [37]. After removal of excess catalase by using the Sephacryl S300 column, its loading efficiency was determined to be 28% according to the standard BCA protein assay. Under transmission electron microscopy (TEM) imaging, the obtained CAT@Pt(IV)-liposome showed a spherical-like structure with an average size of ~100 nm (**Figure 2a**). Moreover, by utilizing the dynamic light scattering (DLS), we found that the size of such CAT@Pt(IV)-liposome was ~100 nm, similar to that of as-prepared Pt(IV)-liposome without the encapsulation of catalase (**Figure 2b**).

Then, the catalytic ability of CAT@Pt(IV)-liposome was carefully studied by using the Góth method and a portable dissolved oxygen meter [34, 38, 40]. It was found that the obtained CAT@Pt(IV)-liposome (catalase = 0.96 μg mL^{-1}) could significantly increase the concentrations of dissolved O$_2$ in the H$_2$O$_2$ solution (1 mM) from 8.85 μg mL^{-1} to 17.27 μg mL^{-1}, while Pt(IV)-liposome under the same Pt concentration did not show any obvious influence on the dissolved O$_2$ concentration in the H$_2$O$_2$ solution (**Figure 2c**), indicating that the catalytic activity of such CAT@Pt(IV)-liposome is originated from the encapsulated catalase. As expected, such CAT@Pt(IV)-liposome showed a catalase concentration dependent catalytic activity towards H$_2$O$_2$ decomposition (**Figure 2d**). By using the Góth method, we found that the catalytic activity of such CAT-Pt(IV)-liposome was ~93% compared to that of free catalase under the same concentration of catalase. Considering the existing of proteases in physiological environments especially in vivo, we

thus wondered whether the liposome encapsulation could protect the catalytic activity of catalase. Under the protease K digestion assay [34, 41], it was found that CAT@Pt(IV)-liposome (catalase = 3.25 µg mL^{-1}) maintained 81% of its initial catalytic activity after being treated with protease K (0.5 mg mL^{-1}) at 37 ^{o}C for 8 h, in marked contrast to free catalase which showed only 35% of retained catalytic activity under the same digestion condition (**Figure 2e&f**). Our results collectively indicate that the liposomal encapsulation of catalase while retaining the catalytic activity of this enzyme could protect it from protease-mediated digestion.

3.2. In vitro cellular uptake and cytotoxicity of CAT@Pt(IV)-liposome

Next, we carefully studied the intracellular internalization and in vitro cytotoxicity of CAT@Pt(IV)-liposome. Under the CLSM, it was found that CAT@Pt(IV)-liposome with CAT labeled by fluorescein (FITC) could be internalized into 4T1 cells via the endocytosis pathway after being incubated at 37 ^{o}C for 2 h, as indicated by the its co-localized fluorescence with intracellular lysosomes (**Figure 3b**). Then, the cytotoxicity of CAT@Pt(IV)-liposome was compared with Pt(IV)-liposome and cisplatin by using the standard cell viability assay. After being incubated with 4T1 cells for 48 h, CAT@Pt(IV)-liposome and its counterpart Pt(IV)-liposome both showed Pt(IV)-concentration dependent cytotoxicity towards cancer cells (**Figure 3c**).

Next, we determined the radiation enhancement ability of CAT-loaded liposomes at the in vitro level. Considering the complex long-term mechanism of released cisplatin pro-drug after X-ray radiation treatment, we only tested CAT@liposome group in clonogenic survival assay to clarify the influence of tumor hypoxia relief on the therapeutic effect of radiation therapy. During clonogenic

survival assay, 4T1 cells were exposed to X-ray at doses of 0 Gy, 2 Gy, 4 Gy, or 6 Gy, in the absence

or presence of CAT@liposome. At the same radiation dose, the survived fraction of 4T1 cells

incubated with CAT@liposome appeared to be obviously lower compared to those without

CAT@liposome incubation, suggesting the capability of CAT@liposome to enhance X-ray induced

cancer cell killing (**Figure S1**).

After that, the capacity of CAT@Pt(IV)-liposome in enhancing the effect of radiotherapy under

the hypoxic environment (cultured under 1% oxygen) was evaluated in vitro by utilizing the

immunocytochemistry staining assay to visualize γ-H2AX, a maker of DNA double-strand damages.

Under the CLSM observation, it was found that the cells treated with CAT@Pt(IV)-liposome plus

X-ray showed the strongest fluorescence signals of γ-H2AX inside cell nuclei compared to those

cells treated with bare CAT@Pt(IV)-liposome, Pt(IV)-liposome and CAT@liposome in the presence

or absence of X-ray (doses: Pt: 15 μg mL^{-1}, X-ray: 6 Gy, **Figure 3d**). By semi-quantitatively

analyzing the γ-H2AX foci densities (γ-H2AX foci/100 μm^2), we found that those cells under

hypoxia after being treated with CAT@Pt(IV)-liposome and CAT@liposome in the presence of

X-ray exposure showed obviously enhanced γ-H2AX foci densities compared to their respective

counterparts without X-ray exposure. However, the X-ray exposure would not significantly improve

the γ-H2AX foci formation in those hypoxic cells treated with bare Pt(IV)-liposome (**Figure 3e**).

Collectively, these results indicate that CAT could efficiently overcome the intrinsic

hypoxia-associated resistance of tumor cells to radiation-induced damages.

3.3. In vivo behaviors of CAT@Pt(IV)-liposome

Afterwards, we studied the in vivo behaviors of CAT@Pt(IV)-liposome by labeling those liposomes with DiD, a widely used hydrophobic fluorescent dye inserted into the lipid bilayer of liposomes for in vivo tracking. Under an in vivo fluorescent imaging system, 4T1 tumor bearing mice with i.v. injection of CAT@Pt(IV)-DiD-liposome (Pt: 3.3 mg kg^1) showed gradually increased fluorescence signals from the tumor over an observation process of 36 h (**Figure 4a&b**). Then, the mice with CAT@Pt(IV)-DiD-liposome injection were sacrificed to study its detailed biodistribution profile. It was found that the tumor showed a high fluorescence signal, which was even obviously stronger than that in the liver though a little weaker than that in the spleen, while the other main organs (e.g. heart, lung, kidney) showed low fluorescence signals (**Figure 4c&d**). Therefore, such CAT@Pt(IV)-DiD-liposome with long blood half-lives ($t_{1/2(\alpha)} = 0.59 \pm 0.24$ h, $t_{1/2(\beta)} = 14.2 \pm 8.67$ h) similar to stealth PEGylated liposomes has a high tumor accumulation ability owing to the enhanced permeability and retention (EPR) effect (**Figure S2**) [37, 42].

Then, the effect of CAT@Pt(IV)-liposome injection on the in vivo tumor hypoxia status was evaluated by ex vivo immunofluorescent staining with pimonidazole as the exogenous hypoxia staining probe and hypoxia induced factor 1α (HIF-1α) protein as the endogenous hypoxia reporter [30]. A total of 12 mice bearing 4T1 tumors were randomly divided into four groups and then received i.v. injection of PBS, Pt(IV)-liposome, CAT@liposome or CAT@Pt(IV)-liposome (doses: CAT = 2 mg kg^{-1}; Pt = 3.3 mg kg^{-1}). At 24 h p.i., all mice were i.p. injected with pimonidazole (0.6 mg per mouse), and sacrificed 90 min later to collect the tumors for cryo-section and immunofluorescent staining to visualize hypoxia signals from pimonidazole. It was found that the tumors on mice treated with i.v. injection of CAT@liposome and CAT@Pt(IV)-liposome showed remarkably relieved hypoxia compared to those treated with i.v. injection of PBS or Pt(IV)-liposome

(**Figure 4e**). By semi-quantitative analysis of hypoxia positive signals in those tumor slices, we found that the percentages of hypoxia positive areas were dramatically decreased from 85.5 and 76.9 % for those treated with i.v. injection of saline and Pt(IV)-liposome, respectively, to 13.69 and 11.45 % for those treated with i.v. injection of CAT@liposome and CAT@Pt(IV)-liposome, respectively (**Figure 4f**). Similarly, the expression levels of HIF-1α protein of tumors collected from mice 24 h after i.v. injection of CAT@liposome or CAT@Pt(IV)-liposome also showed significant decrease (**Figure S3**). Collectively, our results suggest that catalase after being delivered into the tumor by liposomes could efficiently relieve the tumor hypoxia via the decomposition of endogenic H_2O_2 in the tumor microenvironment. Note that although previous reports have uncovered the ability of cisplatin to relieve tumor hypoxia via normalization tumor blood vasculature [43], bare Pt(IV)-liposome at our currently used dose showed no significant effect on tumor hypoxia relief.

3.4. In vivo chemo-radiotherapy cancer therapy

Next, we evaluated the synergistic therapeutic effect of CAT@Pt(IV)-liposome with X-ray radiation on in vivo mouse tumor models. 35 Mice bearing 4T1 tumors with sizes of ~200 mm^3 were randomly divided into seven groups (5 mice per group) as follows: I) control group with PBS injection only; II) bare chemotherapy group with Pt(IV)-liposome injection only; III) CAT@Pt(IV)-liposome injection only; IV) bare radiotherapy group with X-ray exposure only; V) Pt(IV)-liposome injection plus X-ray exposure; VI) CAT@liposome injection plus X-ray exposure; VII) CAT@Pt(IV)-liposome injection plus X-ray exposure. In our experiments, all mice received twice i.v. injections of various agents. At 24 h post injection, the mice from group IV-VII were

exposed to X-ray (6 Gy). The dose of CAT and Pt were 2 mg kg^{-1} and 3.3 mg kg^{-1}, respectively. Then, the tumor sizes were carefully measured with a digital caliper for 14 days. It was found that the treatment of CAT@Pt(IV)-liposome injection plus X-ray exposure (group VII) offered the most effective inhibition effect on tumor growth over all other control groups. Moreover, compared to the treatment by X-ray exposure only (group IV), which showed moderate inhibition effect on tumor growth, treatments by Pt(IV)-liposome injection plus X-ray exposure (group V) and CAT@liposome injection plus X-ray exposure (group VI) appeared to be more effective in tumor growth regression, though not as effective as that achieved in group VII. However, chemotherapy alone by either Pt(IV)-liposome (group II) or CAT@Pt(IV)-liposome was found to be not so effective in delaying the tumor growth, especially at later time points (**Figure 5b**), owing to the relatively low doses of chemotherapeutics used in this experiment.

To further evaluate the cancer treatment efficacy of such hypoxia-relieved chemo-radiotherapy with CAT@Pt(IV)-liposome, the histological changes of tumors were analyzed in detail by utilizing hematoxylin and eosin (H&E) staining assay at day 4. Based on H&E staining, we observed the most severe morphology changes and necrosis for tumor slices collected from the group VII, while moderate damages were observed on those slices in group IV, V, and VI (**Figure 5c**). Collectively, our results indicate that the combined chemo-radiotherapy delivered by CAT@Pt(IV)-liposome with the tumor hypoxia relief function is an effective approach for cancer treatment.

4. Conclusion

In this study, a multifunctional liposomal nanoagent containing CAT and cisplatin prodrug

conjugated phospholipid has been prepared and found to be promising for synergistic cancer chemo-radiotherapy. The obtained CAT@Pt(IV)-liposome shows retained and well-protected catalytic activity to trigger H_2O_2 decomposition. Upon being i.v. injected, such CAT@Pt(IV)-liposome is able to efficiently accumulate in tumors and thereby remarkably relieve the tumor hypoxia via triggering decomposition of tumoral endogenous H_2O_2. After being concurrently applied with X-ray exposure, CAT@Pt(IV)-liposome would contribute to the most effective synergistic tumor growth inhibition effect compared to the respective mono-therapies, as well as the combined chemo-radiotherapy using Pt(IV)-liposome without encapsulating CAT. Our CAT@Pt(IV)-liposome as a multifunctional 'nano-reactor' for tumor hypoxia relief and chemo-radiotherapy is featured with a number of unique advantages: I) The fabrication process of liposomes is rather straightforward and the components of such liposomal nano-agent are fully biocompatible; II) The liposome encapsulation is able to not only retain and protect the catalytic activity of enzyme, but also deliver CAT enzyme into tumors with a high efficiency; III) The efficient tumor hypoxia relief capacity such CAT@Pt(IV)-liposome is robust in overcoming the intrinsic hypoxia associated resistance to both radiotherapy and chemo-radiotherapy. However, tremendous additional efforts are still demanded to test the efficacy of our liposomal nanoparticles in more advanced & clinically relevant animal tumor models. Nevertheless, our work presents a multifunctional liposomal nano-agent promising for further clinical translation in combined chemo-radiotherapy treatment of cancers.

Supporting Information

Supporting Information is available from the Wiley Online Library or from the author.

References

[1] DeSanto. Induction Chemotherapy plus Radiation Compared with Surgery plus Radiation in Patients with Advanced Laryngeal Cancer. New Engl. J. Med. 1991;324:1685-90.

[2] Jr DVV, Chu E. A history of cancer chemotherapy. Cancer Res. 2008;68:8643-53.

[3] D'Amico AV, Whittington R, Malkowicz SB, Schultz D, Blank K, Broderick GA, et al. Biochemical outcome after radical prostatectomy, external beam radiation therapy, or interstitial radiation therapy for clinically localized prostate cancer. J. Am. Med. Assoc. 1998;280:969-74.

[4] Al-Sarraf M, Leblanc M, Giri PG, Fu KK, Cooper J, Vuong T, et al. Chemoradiotherapy versus radiotherapy in patients with advanced nasopharyngeal cancer: phase III randomized Intergroup study 0099. J. Clin. Oncol. 1998;16:1310-7.

[5] Poon MA. Chemoradiotherapy after Surgery Compared with Surgery Alone for Adenocarcinoma of the Stomach or Gastroesophageal Junction. New Engl. J. Med. 2001;345:725-30.

[6] Stocken DD. A Randomized Trial of Chemoradiotherapy and Chemotherapy after Resection of Pancreatic Cancer. New Engl. J. Med. 2004;350:1200-10.

[7] Forastiere AA, M.D, Goepfert H, M.D, Maor M, M.D, et al. Concurrent Chemotherapy and Radiotherapy for Organ Preservation in Advanced Laryngeal Cancer. New Engl. J. Med. 2003;349:2091-8.

[8] Lawrence TS, Blackstock AW, Mcginn C. The mechanism of action of radiosensitization of conventional chemotherapeutic agents. Semin. Radiat. Oncol. 2003;13:13-21.

[9] Rose PG, Bundy BN, Watkins EB, Thigpen JT, Deppe G, Maiman MA, et al. Concurrent cisplatin-based radiotherapy and chemotherapy for locally advanced cervical cancer. New Engl. J. Med. 1999;340:1144-53.

[10] Eramo A, Riccivitiani L, Zeuner A, Pallini R, Lotti F, Sette G, et al. Chemotherapy resistance of glioblastoma stem cells. Cell Death. Differ. 2006;13:1238-41.

[11] Pommier Y, Sordet O, Antony S, Hayward RL, Kohn KW. Apoptosis defects and chemotherapy resistance: Molecular maps and networks. Oncogene 2004;23:2934-49.

[12] Harrison L, Blackwell K. Hypoxia and anemia: factors in decreased sensitivity to radiation therapy and chemotherapy? Oncologist 2004;9:31-40.

[13] Harada H. How Can We Overcome Tumor Hypoxia in Radiation Therapy? J. Radiat. Res. 2011;52:545-56.

[14] Kondo A SR, M M. Hypoxia-induced enrichment and mutagenesis of cells that have lost DNA mismatch repair. Cancer Res. 2001;61:7603-7.

[15] Moeller BJ, Richardson RA, Dewhirst MW. Hypoxia and radiotherapy: opportunities for improved outcomes in cancer treatment. Cancer Metast. Rev. 2007;26:241-8.

[16] Brown JM, Wilson WR. Exploiting tumour hypoxia in cancer treatment. Nat. Rev. Cancer 2004;4:437-47.

[17] Vaupel P, Kelleher DK, Höckel M. Oxygen status of malignant tumors: pathogenesis of hypoxia and significance for tumor therapy. Semin. Oncol. 2001;28:29-35.

[18] Y Liu, Y Liu, W Bu, Q Xiao, Y Sun, K Zhao, et al. Radiation-/hypoxia-induced solid tumor metastasis and regrowth inhibited by hypoxia-specific upconversion nanoradiosensitizer. Biomaterials 2015;49:1-8.

[19] Abbasi AZ, Gordijo CR, Amini MA, Maeda A, Rauth AM, Dacosta RS, et al. Hybrid manganese dioxide nanoparticles potentiate radiation therapy by modulating tumor hypoxia. Cancer Res. 2016;76:1-14.

[20] Prasad P, Gordijo CR, Abbasi AZ, Maeda A, Ip A, Rauth AM, et al. Multifunctional albumin-MnO_2 nanoparticles modulate solid tumor microenvironment by attenuating hypoxia, acidosis, vascular endothelial growth factor and enhance radiation response. ACS Nano 2014;8:3202-12.

[21] Chen H, He W, Guo Z. An H_2O_2-responsive nanocarrier for dual-release of platinum anticancer drugs and O_2: controlled release and enhanced cytotoxicity against cisplatin resistant cancer cells. Chem. Commun. 2014;50:9714-7.

[22] Fan W, Bu W, Shen B, He Q, Cui Z, Liu Y, et al. Intelligent MnO_2 Nanosheets Anchored with Upconversion Nanoprobes for Concurrent pH‐/H_2O_2‐Responsive UCL Imaging and Oxygen‐Elevated Synergetic Therapy. Adv. Mater. 2015;27:4155-61.

[23] Fan W, Bu W, Zhang Z, Shen B, Zhang H, He Q, et al. X-ray Radiation-Controlled NO-Release for On-Demand Depth-Independent Hypoxic Radiosensitization. Angew. Chem. Int. Ed. 2015;54:14026.

[24] Liu Y, Liu Y, Bu W, Cheng C, Zuo C, Xiao Q, et al. Hypoxia Induced by Upconversion-Based Photodynamic Therapy: Towards Highly Effective Synergistic Bioreductive Therapy in Tumors. Angew. Chem. Int. Ed. 2015;54:8105-9.

[25] Verwilst P, Han J, Lee J, Mun S, Kang HG, Kim JS. Reconsidering azobenzene as a component of small-molecule hypoxia-mediated cancer drugs: A theranostic case study. Biomaterials 2016;115:104-14.

[26] Kumar R, Kim EJ, Han J, Lee H, Shin WS, Kim HM, et al. Hypoxia-directed and activated theranostic agent: Imaging and treatment of solid tumor. Biomaterials 2016;104:119-28.

[27] Cheng L, Shen S, Shi S, Yi Y, Wang X, Song G, et al. $FeSe_2$‐Decorated Bi_2Se_3 Nanosheets Fabricated via Cation Exchange for Chelator‐Free ^{64}Cu‐Labeling and Multimodal Image‐Guided Photothermal‐Radiation Therapy. Adv. Funct. Mater. 2016;26:2185-97.

[28] Song G, Liang C, Gong H, Li M, Zheng X, Cheng L, et al. Core-Shell $MnSe@Bi_2Se_3$ Fabricated via a Cation Exchange Method as Novel Nanotheranostics for Multimodal Imaging and Synergistic Thermoradiotherapy. Adv. Mater. 2015;27:6110-7.

[29] Song G, Liang C, Yi X, Zhao Q, Cheng L, Yang K, et al. Perfluorocarbon‐Loaded Hollow Bi2Se3 Nanoparticles for Timely Supply of Oxygen under Near‐Infrared Light to Enhance the Radiotherapy of Cancer. Adv. Mater. 2016;28:2716-23.

[30] Song X, Feng L, Liang C, Yang K, Liu Z. Ultrasound Triggered Tumor Oxygenation with Oxygen-Shuttle Nanoperfluorocarbon to Overcome Hypoxia-Associated Resistance in Cancer Therapies. Nano. Lett. 2016;16:6145-53.

[31] Yi X, Chen L, Zhong X, Gao R, Qian Y, Wu F, et al. Core–shell $Au@MnO_2$ nanoparticles for

enhanced radiotherapy via improving the tumor oxygenation. Nano Res. 2016;9:1-12.

[32] Gong H, Yu C, Xiang J, Han X, Song G, Feng L, et al. Hyaluronidase To Enhance Nanoparticle-Based Photodynamic Tumor Therapy. Nano Lett. 2016;16:2512-21.

[33] Luo Z, Zheng M, Zhao P, Chen Z, Siu F, Ping G, et al. Self-Monitoring Artificial Red Cells with Sufficient Oxygen Supply for Enhanced Photodynamic Therapy. Sci. Rep. 2016;6:23393.

[34] Song G, Chen Y, Liang C, Yi X, Liu J, Sun X, et al. Catalase‐Loaded TaOx Nanoshells as Bio‐Nanoreactors Combining High‐Z Element and Enzyme Delivery for Enhancing Radiotherapy. Adv. Mater. 2016;28:7143-8.

[35] Lebwohl D, Canetta R. Clinical development of platinum complexes in cancer therapy: an historical perspective and an update. Eur. J. Cancer. 1998;34:1522-34.

[36] Boulikas T, Vougiouka M. Cisplatin and platinum drugs at the molecular level. Oncol. Rep. 2003;10:1663-82.

[37] Feng L, Gao M, Tao D, Chen Q, Wang H, Dong Z, et al. Cisplatin‐Prodrug‐Constructed Liposomes as a Versatile Theranostic Nanoplatform for Bimodal Imaging Guided Combination Cancer Therapy. Adv. Funct. Mater. 2016;26:2207-17.

[38] Góth L. A simple method for determination of serum catalase activity and revision of reference range. Clin Chim Acta 196: 143-152. Clin. Chim. Acta. 1991;196:143-51.

[39] Shi J, Kantoff PW, Wooster R, Farokhzad OC. Cancer nanomedicine: progress, challenges and opportunities. Nat. Rev. Cancer 2016;17:20-37.

[40] Yang X, Cai Z, Ye Z, Chen S, Yang Y, Wang H, et al. In situ synthesis of porous silica nanoparticles for covalent immobilization of enzymes. Nanoscale 2011;4:414-6.

[41] Southan C, Williams AJ, Ekins S. Challenges and recommendations for obtaining chemical structures of industry-provided repurposing candidates. Drug Discov. Today 2013;18:58-70.

[42] Song X, Feng L, Liang C, Gao M, Song G, Liu Z. Liposomes co-loaded with metformin and chlorin e6 modulate tumor hypoxia during enhanced photodynamic therapy. Nano Res. 2016:1-13.

[43] Duyndam MC, van Berkel MP, Dorsman JC, Rockx DA, Pinedo HM, Boven E. Cisplatin and doxorubicin repress Vascular Endothelial Growth Factor expression and differentially down-regulate Hypoxia-inducible Factor I activity in human ovarian cancer cells. Biochem. Pharmacol. 2007;74:191-201.

Figure 1. A scheme showing the preparation of CAT@Pt(IV)-liposome for tumor hypoxia relieved cancer chemo-radiotherapy. The molar ratio of DSPE-Pt(IV), DPPC, cholesterol and DSPE-PEG was 8:8:4:1.

Figure 2. Characterization of CAT@Pt(IV)-liposome. (a) TEM image and (b) DLS measurement of CAT@Pt(IV)-liposome. (c) The O_2 concentration changes in H_2O_2 solutions (1 mM) with addition of Pt(IV)-liposome and CAT@Pt(IV)-liposome measured by a portable dissolved oxygen meter. (d) The O_2 concentration changes in H_2O_2 solutions (1 mM) after incubation with CAT@Pt(IV)-liposome at indicated CAT concentrations. (e) The relative enzymatic activity changes of free catalase and CAT@Pt(IV)-liposome under protease K digestion (0.5 mg mL^{-1}) for different periods of times. (f) Photograph showing the O_2 production of free catalase and CAT@Pt(IV)-liposome in H_2O_2 solutions before and after protease K digestion for 24 h.
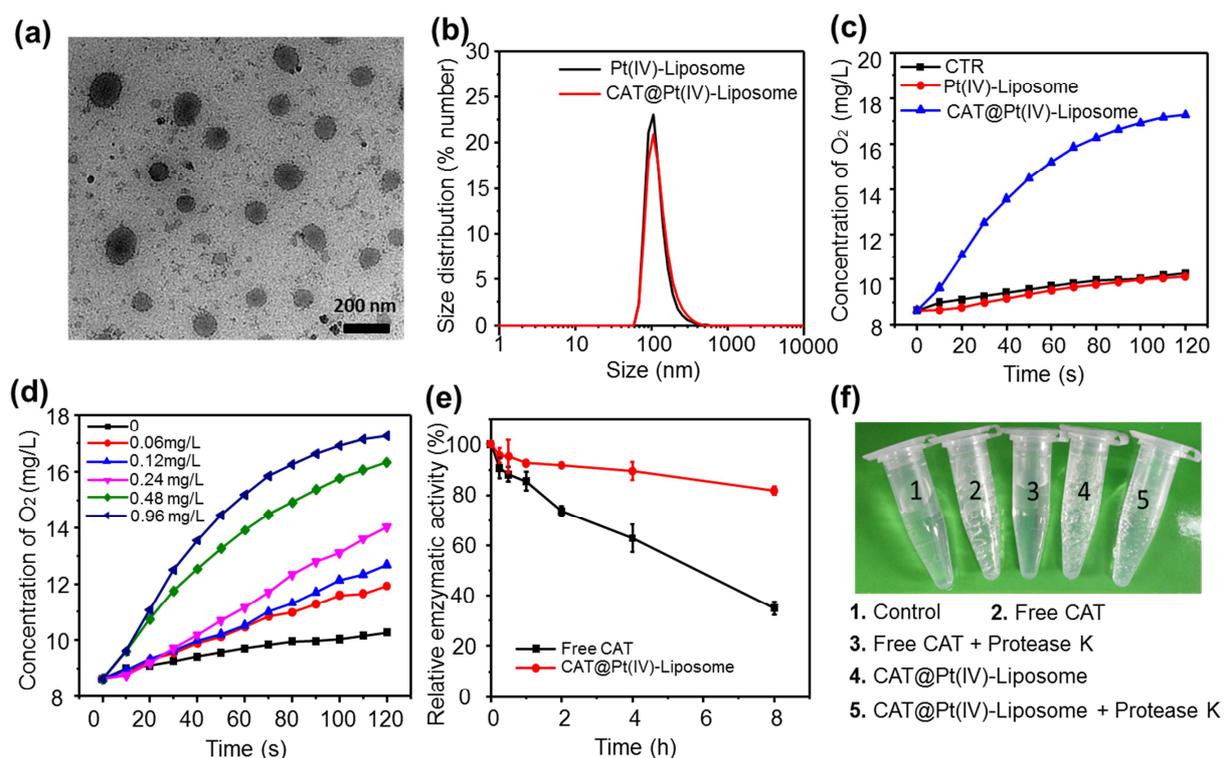
Figure 3. In vitro cellular uptake and cytotoxicity of CAT@Pt(IV)-liposome. (a) A scheme showing that CAT@Pt(IV)-liposome could efficiently relieve tumor hypoxia and then contribute to enhanced chemo-radiotherapy. (b) Intracellular internalization of FITC-CAT@Pt(IV)-liposome into 4T1 cells imaged by the CLSM. (c) Relative viabilities of 4T1 cells treated with cisplatin, cisplatin + catalase, Pt(IV)-liposome and CAT@Pt(IV)-liposome at a series of Pt concentrations for 48 h, measured by the standard MTT assay. (d) γ-H2AX staining showing the DNA double strand break status of those 4T1 cancer cells treated with Pt(IV)-liposome, CAT@liposome and CAT@Pt(IV)-liposome with or without X-ray exposure. The dose of X-ray radiation was 6 Gy. The concentrations of Pt and catalase were 15 μg mL^{-1} and 9 μg mL^{-1}, respectively. (e) Semi-quantitative analysis of γ-H$_2$AX foci density (γ-H$_2$AX foci/100 μm^2) for 100 cells in each treatment group with the Image J software. P values were calculated by the Student's t-test: ***$P < 0.001$ (n = 100).

Figure 4. In vivo behaviors of CAT@Pt(IV)-liposome. (a) Time-lapsed in vivo fluorescence imaging of 4T1 tumor-bearing mice with i.v. injection of CAT@Pt(IV)-DiD-liposome. The tumors were indicated with the black dashed circles. (b) Semi-quantitative analysis of tumor fluorescence signals based on the images shown in (a). (c) Ex vivo fluorescence images of the major organs/tissues collected from the mice with i.v. injection of CAT@Pt(IV)-DiD-liposome. Li, Sp, Ki, He, Lu, and Tu stand for liver, spleen, kidney, heart, lung and tumor, respectively. (d) Semi-quantitative analysis of fluorescence signals of each organ / tissue based on the image shown in (c). (e) Ex vivo immunofluorescence staining of tumor slices collected from mice with i.v. injection of saline, Pt(IV)-liposome, CAT@liposome, or CAT@Pt(IV)-liposome at 24 h p.i. The cell nuclei, blood vessels, and hypoxia areas stained with DAPI (blue), anti-CD31 antibody (red), and hypoxia-probe (green), respectively. (f) Semi-quantitative analysis of positive tumor hypoxia areas based on the images shown in (e) by using the Image J software (n = 5 images per group).
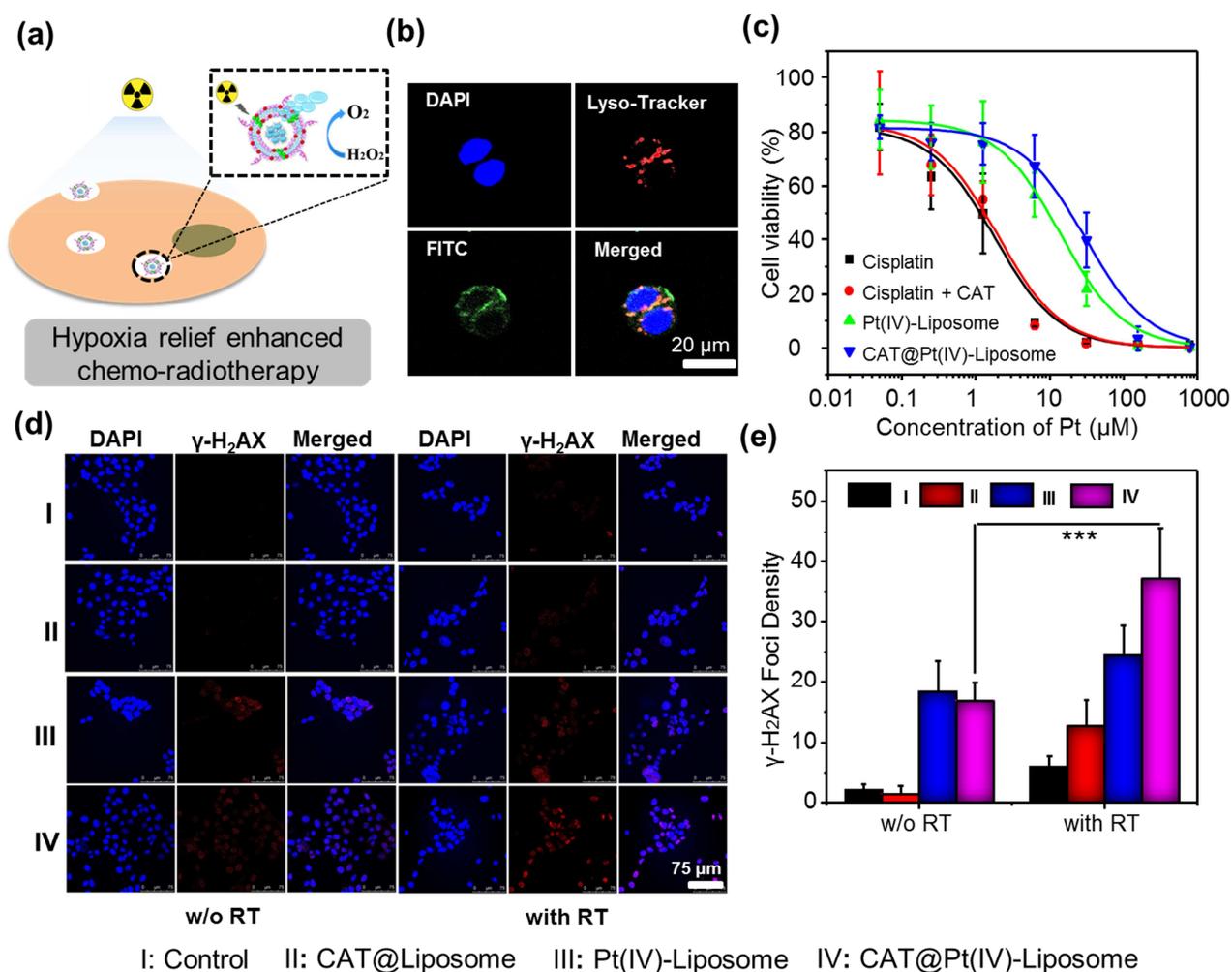
Figure 5. In vivo chemo-radiotherapy cancer therapy. (a) A scheme showing combined chemo-radiotherapy with CAT@Pt(IV)-liposome. (b) Tumor growth curves of mice after various

different treatments indicated. V and V_o stand for the tumor volumes after and before the treatment, respectively. Error bars were based on five mice in each group. All mice received twice injections of indicated materials at day -1 and day 2 and then were exposed to X-ray radiation at 24 h p.i. Day 0 refers to the day that the first dose X-ray radiation was applied. The doses of Pt and catalase were 3.3 and 2 mg kg^{-1}, respectively, the dose of X-ray was 6 Gy. (c) Micrographs of H&E-staining of tumor slices collected from mice of different groups at day 4. The combined chemo-radiotherapy with CAT@Pt(IV)-liposome resulted in the most significant damages to tumor cells. P values were calculated by the Student's t-test: $*P < 0.1$, $**P < 0.01$ (n = 5).

Figure 1. A scheme showing the preparation of CAT@Pt(IV)-liposome for tumor hypoxia relieved cancer chemo-radiotherapy. The molar ratio of DSPE-Pt(IV), DPPC, cholesterol and DSPE-PEG was 8:8:4:1.
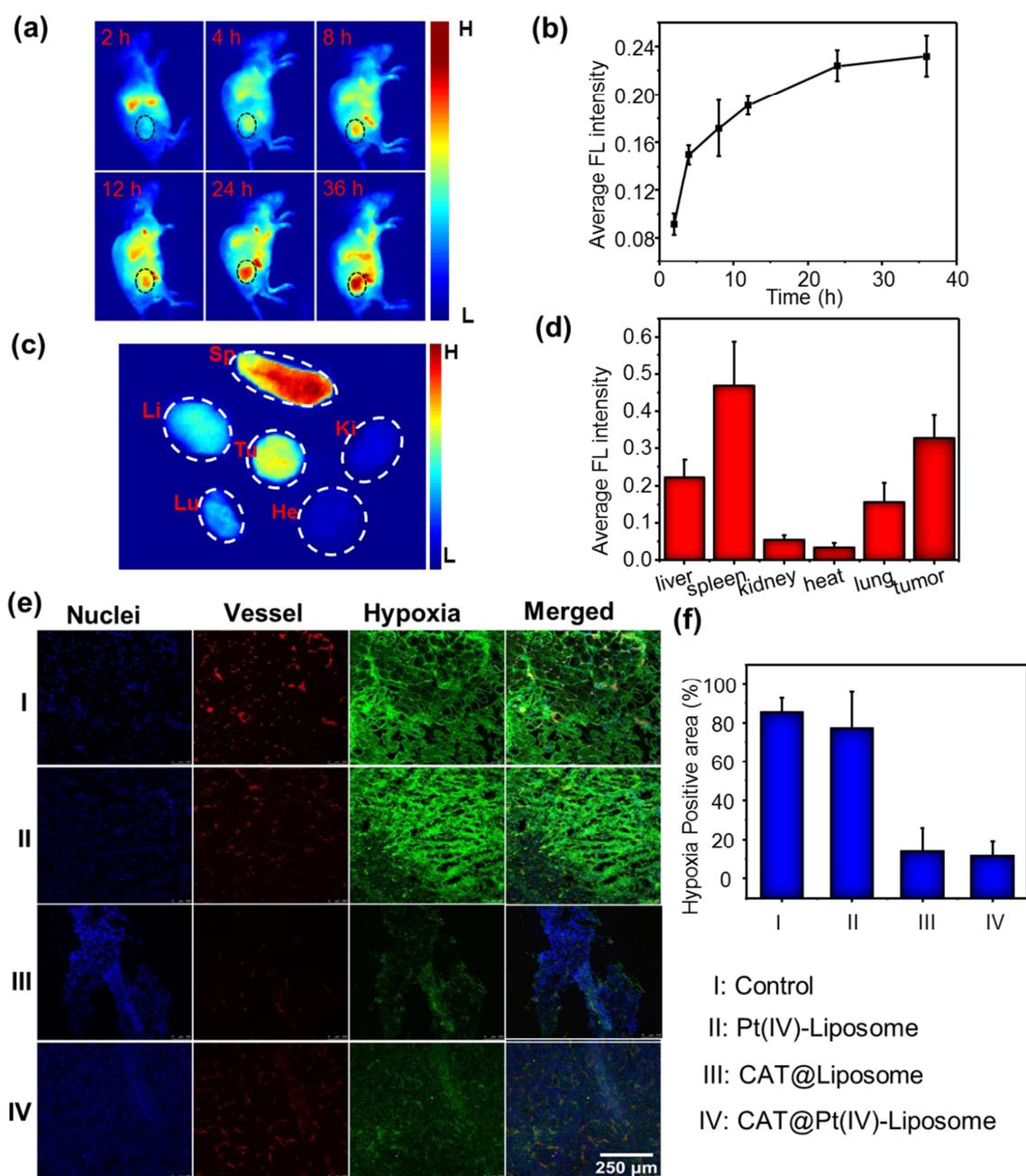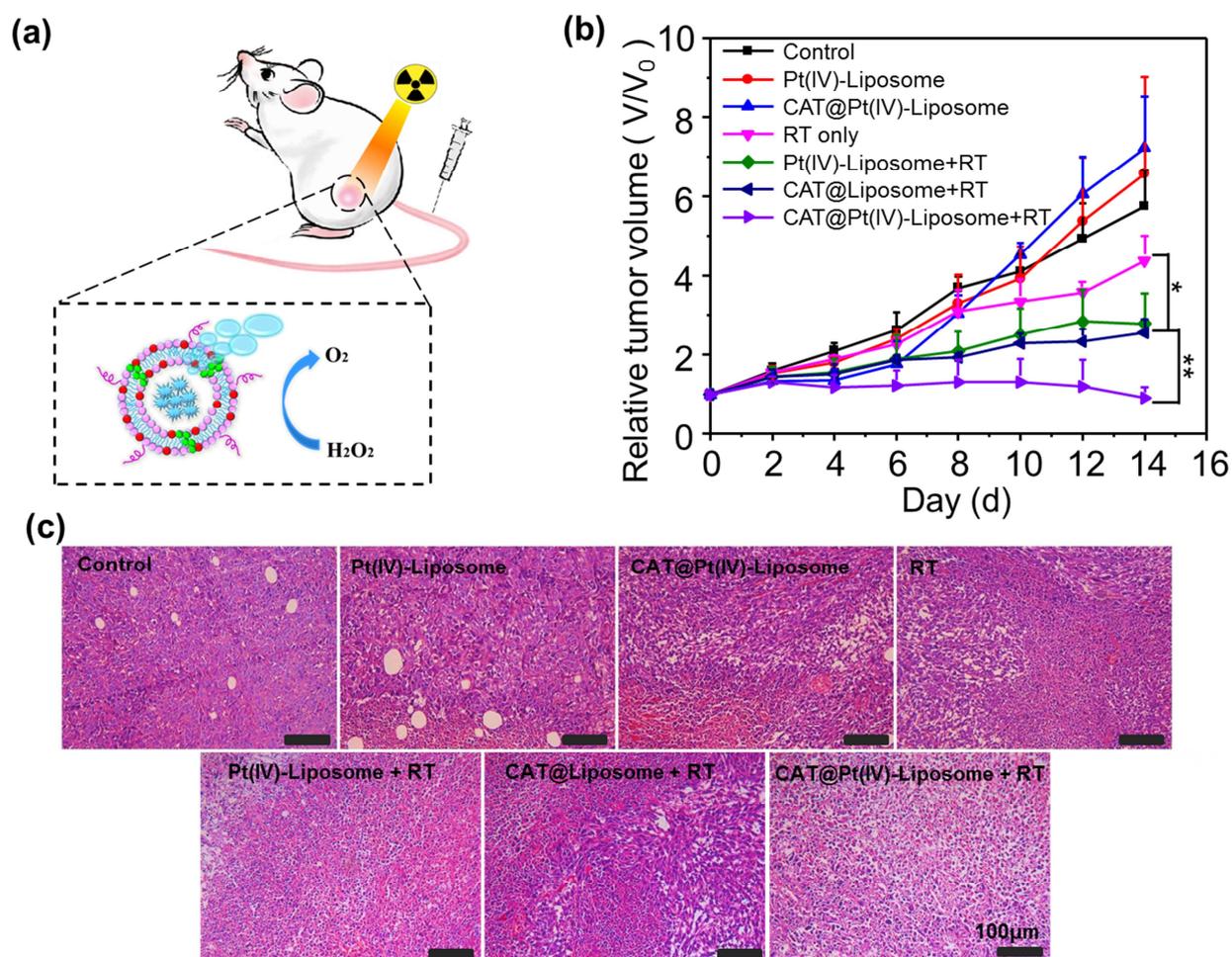
Figure 2. Characterization of CAT@Pt(IV)-liposome. (a) TEM image and (b) DLS measurement of CAT@Pt(IV)-liposome. (c) The O_2 concentration changes in H_2O_2 solutions (1 mM) with addition of Pt(IV)-liposome and CAT@Pt(IV)-liposome measured by a portable dissolved oxygen meter. (d) The O_2 concentration changes in H_2O_2 solutions (1 mM) after incubation with CAT@Pt(IV)-liposome at indicated CAT concentrations. (e) The relative enzymatic activity changes of free catalase and CAT@Pt(IV)-liposome under protease K digestion (0.5 mg mL^{-1}) for different periods of times. (f) Photograph showing the O_2 production of free catalase and CAT@Pt(IV)-liposome in H_2O_2 solutions before and after protease K digestion for 24 h.

Figure 3. In vitro cellular uptake and cytotoxicity of CAT@Pt(IV)-liposome. (a) A scheme showing that CAT@Pt(IV)-liposome could efficiently relieve tumor hypoxia and then contribute to enhanced chemo-radiotherapy. (b) Intracellular internalization of FITC-CAT@Pt(IV)-liposome into 4T1 cells imaged by the CLSM. (c) Relative viabilities of 4T1 cells treated with cisplatin, cisplatin + catalase, Pt(IV)-liposome and CAT@Pt(IV)-liposome at a series of Pt concentrations for 48 h, measured by the standard MTT assay. (d) γ-H2AX staining showing the DNA double strand break status of those 4T1 cancer cells treated with Pt(IV)-liposome, CAT@liposome and CAT@Pt(IV)-liposome with or without X-ray exposure. The dose of X-ray radiation was 6 Gy. The concentrations of Pt and catalase were 15 μg mL^{-1} and 9 μg mL^{-1}, respectively. (e) Semi-quantitative analysis of γ-H$_2$AX foci density (γ-H$_2$AX foci/100 μm^2) for 100 cells in each treatment group with the Image J software. *P* values were calculated by the Student's *t* -test: ***$P < 0.001$ (n = 100).

Figure 4. In vivo behaviors of CAT@Pt(IV)-liposome. (a) Time-lapsed in vivo fluorescence imaging of 4T1 tumor-bearing mice with i.v. injection of CAT@Pt(IV)-DiD-liposome. The tumors were indicated with the black dashed circles. (b) Semi-quantitative analysis of tumor fluorescence signals based on the images shown in (a). (c) Ex vivo fluorescence images of the major organs/tissues collected from the mice with i.v. injection of CAT@Pt(IV)-DiD-liposome. Li, Sp, Ki, He, Lu, and Tu stand for liver, spleen, kidney, heart, lung and tumor, respectively. (d) Semi-quantitative analysis of fluorescence signals of each organ / tissue based on the image shown in (c). (e) Ex vivo immunofluorescence staining of tumor slices collected from mice with i.v. injection of saline, Pt(IV)-liposome, CAT@liposome, or CAT@Pt(IV)-liposome at 24 h p.i. The cell nuclei, blood vessels, and hypoxia areas stained with DAPI (blue), anti-CD31 antibody (red), and hypoxia-probe (green), respectively. (f) Semi-quantitative analysis of positive tumor hypoxia areas based on the images shown in (e) by using the Image J software (n = 5 images per group).

Figure 5. In vivo chemo-radiotherapy cancer therapy. (a) A scheme showing combined chemo-radiotherapy with CAT@Pt(IV)-liposome. (b) Tumor growth curves of mice after various different treatments indicated. V and V_o stand for the tumor volumes after and before the treatment, respectively. Error bars were based on five mice in each group. All mice received twice injections of indicated materials at day -1 and day 2 and then were exposed to X-ray radiation at 24 h p.i. Day 0 refers to the day that the first dose X-ray radiation was applied. The doses of Pt and catalase were 3.3 and 2 mg kg^{-1}, respectively, the dose of X-ray was 6 Gy. (c) Micrographs of H&E-staining of tumor slices collected from mice of different groups at day 4. The combined chemo-radiotherapy with CAT@Pt(IV)-liposome resulted in the most significant damages to tumor cells. P values were calculated by the Student's t-test: $*P < 0.1$, $**P < 0.01$ (n = 5).